RSC Advances

PAPER

View Article Online
View Journal | View Issue

Cite this: *RSC Adv.*, 2015, **5**, 10094

Using Raman and dielectric spectroscopy to elucidate the spin phonon and magnetoelectric coupling in $DyCrO_3$ nanoplatelets

Preeti Gupta[ab] and Pankaj Poddar*[abc]

Received 23rd September 2014
Accepted 6th January 2015

DOI: 10.1039/c4ra11022f

www.rsc.org/advances

In this study, we report the phonon-mode assignment of $DyCrO_3$ nanoplatelets by Raman spectroscopy. The temperature dependent Raman studies indicate the shift in the phonon frequency of most intense modes of $DyCrO_3$ and the observed change in Raman line-width is correlated with the spin–phonon coupling. The impedance spectroscopy reveals anomalies in the dielectric constant *vs.* temperature curve in the proximity of the magnetic transitions, thereby hinting towards possible weak magnetoelectric coupling in $DyCrO_3$ nanoplatelets. For the first time, UV-vis absorption spectroscopy and photocatalytic activity of $DyCrO_3$ nanoplatelets have been reported. The optical absorption spectrum gives the band gap ~2.8 eV for $DyCrO_3$ nanoplatelets suggesting them as a good candidate for studying photocatalytic activity. The $DyCrO_3$ nanoplatelets showed an efficient photocatalytic activity by degrading 65% methyl orange after 8 h irradiation.

1. Introduction

In the last decade, researchers have shown renewed interest in the search for multiferroic materials with magnetoelectric coupling due to their simultaneous ordering of electrical dipoles and spins. The coexistence of ferro/ferri/antiferromagnetic, ferroelectric, and ferroelastic properties of these materials make them suitable for different applications such as high density data-storage devices, spintronics, magnetoelectric sensors, and lead-free piezoelectrics.[1–5] Few of the these materials show weak magnetoelectric (ME) coupling at much lower temperature than room temperature (RT), in which, the magnetization is controlled by applied electric field or the electric-polarization is controlled by the magnetic field. The spin–lattice coupling in the multiferroic materials contributes significantly to the interplay between the electric-polarization and magnetic ordering. In order to study these features in such materials, it is essential to study the lattice dynamics. In recent years, Raman spectroscopy has emerged as a powerful non-destructive technique to study molecular and crystal lattice vibrations. There are several reports which deal with the Raman studies of multiferroic-materials. Recently, Weber *et al.* studied the phonon-spectra of $RCrO_3$ series, in order to assign the phonon modes associated with it, to get a better understanding of its structure.[6] Feng *et al.* studied the pressure-dependent change in the phase transition temperature in Dy-doped $HoMnO_3$ *via* Raman spectroscopy.[7] In perovskite such as $RMnO_3$, $RFeO_3$, $RNiO_3$, $RCrO_3$ *etc.*, the octahedral tilt angle or the distortion can be tuned by the ionic size of rare earth ion.[8] Among such materials, rare-earth chromites are important class of perovskite materials and they have attracted great attention in past owing to their magnetoelectric properties in addition to the rich and complex magnetic phases at very low temperature.[8–16]

In orthochromites, the interplay between the magnetic and electric order can be understood by considering the spin–lattice coupling phenomenon. Recently, the room-temperature Raman-spectra of $LnCrO_3$ (Y, La, Pr, Sm, Gd, Nd, Dy, Ho, Yb, Er and Lu) have been reported and analyzed based on symmetry associated with the structural distortion.[17–22] The phonon behavior of these multiferroic materials shows an anomaly near Nèel transition temperature in Raman modes.[8] Though, manganites and ferrites have also been studied extensively in past, however, very few reports of Raman studies are reported for chromites.[6,8,18,20]

In addition, the dielectric properties of the rare earth chromites have been studied but they are limited to few $RCrO_3$ (R = Gd, Sm).[8,23] Recently, Prado-Gonjal *et al.* have studied the dielectric properties of submicron-sized $RCrO_3$ particles which include $DyCrO_3$ (DCO) also.[24] However; most of the studies are reported at RT and above, while the magnetic transitions in chromites appear at much lower temperatures.[13,24] Therefore, the relation between dielectric properties and magnetic anomalies is still not investigated in detail for the nanosized DCO as

[a]*Physical & Material Chemistry Division, CSIR-National Chemical Laboratory, Pune – 411008, India. E-mail: p.poddar@ncl.res.in; Fax: +91-20-2590-2636; Tel: +91-20-2590-2580*

[b]*Academy of Scientific and Innovative Research, Anusandhan Bhawan, 2 Rafi Marg, New Delhi – 110 001, India*

[c]*Center of Excellence on Surface Science, CSIR-National Chemical Laboratory, Pune – 411008, India*

this subtle coupling appears at much lower temperature (much below the magnetic transitions). Thus, there is a need to study the temperature and frequency dependence of DCO nanocrystallites and correlate with the interesting magnetic transitions at low temperature.

Though, the interest in this family of compounds (not limited to rare earth chromites) has largely remain confined to study the multiferroic properties, however, recent studies have revealed that the multiferroic materials can be classified as semiconductors rather than insulators.[25] This has attracted further attention to study their photocatalytical and other light-harvesting properties such as solar photovoltaics. Among all the multiferroic material, bismuth ferrite (BFO) has gain a considerable interest in studying its photocatalytic activity due to its favorable band-gap ~2.7 eV. The BFO nanoparticles show enhance photocatalytic properties under UV-visible light irradiation.[26] The rare earth chromites are known to be p-type semiconductors showing electronic sensitivity toward humidity and gases such as H_2, CO, NO, N_2O, and so forth, which is useful for sensor applications.[27,28] Apart from sensing application, doped-$LaCrO_3$ were found to be good candidates as interconnect materials in solid oxide fuel cells.[29] For some doped chromites, catalysis properties toward hydrocarbon oxidation have also been investigated.[30] The rare earth chromites have advantage over conventional photocatalytic materials such as titania as their rich optical nature provides absorption bands in visible range also (in contrast to pure titania).[31] Till date, the photocatalytic study has not been reported on DCO nanocrystallites. In this work, we have tried to explore its optical properties and to study its photocatalytic activity.

In the present work, we report temperature-dependent Raman spectroscopy study in an effort to elucidate the origin of local structural distortion, and spin–phonon coupling in the DCO nanoplatelets. The observed anomaly in the phonon-modes line-width confirms the spin–phonon coupling in DCO nanoplatelets. The modes involving R–O and Cr–O vibrations also show anomalous change in phonon-line-width and phonon-frequency. Below, we also present the detailed study of dielectric-spectroscopy and photocatalytic activity of the DCO nanoplatelets.

2. Experimental and characterization

The DCO nanoplatelets were prepared using the sol–gel technique. The details of sample preparation and characterization are reported elsewhere.[32] Raman spectra were recorded on a HR-800 Raman spectrophotometer (Jobin Yvon-Horiba, France) using monochromatic radiation (achromatic Czerny–Turner type monochromator with silver treated mirrors) emitted by a He–Ne laser (633 nm), operating at 20 mW and with Raman-shift detection accuracy of ± 1 cm^{-1} between 450 nm and 850 nm, equipped with thermoelectrically cooled (with Peltier junctions), multi-channel, spectroscopic-grade CCD detector (1024 × 256 pixels of 26 microns) with dark current lower than 0.002 electrons per pixel per s using a 100× objective. In order to record temperature dependent Raman spectra using cooling–heating stage, the samples were mounted on a LINKAM THMS 600 heating/freezing stage to which a temperature programmer TP 94 was connected with a temperature controller and the temperature varied in the range of 93–300 K with a heating rate of 10 K min^{-1}. To maintain the stage at low temperature, liquid nitrogen was used. Temperature dependent Raman spectra of as-synthesized DCO nanoplatelets were recorded in a temperature range 93–300 K.

For the dielectric measurements, the DCO polycrystallites were pressed into 13 mm circular pellet. To probe the dielectric response in the proximity of magnetic transitions, impedance spectroscopy was carried out in a temperature range 20–300 K using a Novacontrol Beta NB Impedance Analyser with a home-built sample holder coupled with a Janis cryostat. The data were recorded in a frequency range 1 to 10^6 Hz at 1 V (rms). UV-vis-NIR spectroscopy measurements were performed on a Jasco UV-vis-NIR (Model V570) dual beam spectrometer operated at a resolution of ~2 nm. The photocatalytic activity of the DCO nanoplatelets was studied by monitoring the degradation of methyl orange in aqueous medium under UV light using a 400 W mercury lamp. The reaction was carried out at room temperature by circulating cooling water in order to prevent thermal catalytic effect. Prior to the UV illumination, the suspensions were stirred continuously in dark to reach the equilibrium between catalyst and methyl orange (MO) dye. The aqueous suspensions of MO with the concentration of 15 mg L^{-1} and the DCO powder (1.57 g L^{-1}) were placed in a round bottom flask followed by continuous stirring. The degradation of MO was evaluated by centrifuging the retrieved samples and recording the intensity of absorption peak of methyl orange (~462 nm) relative to its initial intensity (C/C_0) using a spectrophotometer.

3. Results and discussion

3.1. Raman studies

Raman scattering is a powerful technique to measure the structural anomaly as it is sensitive to the crystal symmetry. The perovskite DCO has an orthorhombic structure belonging to *Pbnm* space group with four formula units in the primitive cell. The irreducible representation Γ for the *Pbnm* space group of the Raman-active modes at the zone centre can be decomposed[33] and represented as:

$$\Gamma\ (\text{Raman}) = 7A_{1g} + 7B_{1g} + 5B_{2g} + 5B_{3g}$$

These 24 modes are Raman active modes and can be classified as two symmetric ($A_g + B_{1g}$) and four antisymmetric octahedral stretching modes ($2B_{2g} + 2B_{3g}$), four bending modes ($A_g + 2B_{2g} + B_{3g}$), and six rotation or tilt modes of the octahedral ($2A_g + B_{1g} + 2B_{2g} + B_{3g}$). The other eight modes are usually associated with the dysprosium cation movement ($3A_g + 3B_{1g} + B_{2g} + B_{3g}$).[33] However, this space group also consists of other 25 optical modes which include 8 optical modes with symmetry A_u, and three acoustic modes. These 36 modes are not Raman

active. The irreducible representation for these modes can be done as:[33,34]

$$\Gamma\ (\mathrm{IR}) = 9\mathrm{B_{1u}} + 7\mathrm{B_{2u}} + 9\mathrm{B_{2u}}$$

$$\Gamma\ (\mathrm{acoustic}) = \mathrm{B_{1u}} + \mathrm{B_{2u}} + \mathrm{B_{2u}}$$

$$\Gamma\ (\mathrm{silent}) = 8\mathrm{A_u}$$

Weber *et al.* assigned these modes by following various previous reports on Raman spectroscopy on $RCrO_3$ family of compounds.[6] The structural distortion from the parent cubic perovskite structure may result from (i) the rotation of CrO_6 octahedra along [010] and [101] axes, (ii) displacement of Dy^{3+} along certain direction, and (iii) the Jahn–Teller (J–T) distortion.[35] Cr^{3+} ion is a Jahn–Teller (JT) in-active cation and no dispersion in the Cr–O bonds are expected. Such distortion (tilt, octahedra distortion and A-cation displacement) breaks the cubic symmetry in the perovskite and cannot be detected by simple diffraction techniques, but it is possible to study by Raman spectroscopy.

In the present study, we try to assign symmetry to the phonon modes based on orthorhombic structure with space group of *Pbnm* using RT Raman spectroscopy study.[19,36,37] Fig. 1 represents the RT-Raman spectra of DCO nanoplatelets in the spectral range 100–800 cm^{-1} showing prominent Raman modes near ~295, 346, 427, 488, 547, 602, and 707 cm^{-1}. The modes involving Dy^{3+} atomic vibration show-up at lower wavenumber, below 200 cm^{-1}.[6] In the region above 200 cm^{-1}, phonon modes at 265 and 300 cm^{-1} correspond to the in-phase and out-of-phase octahedral rotation around *y*-axis. The doublets observed around ~346 cm^{-1} (A_g and B_{2g}) are related to the R–O vibration. The phonon modes, A_g and B_{1g}, at ~429 cm^{-1} are associated with the in-phase and out-of-phase octahedral rotation around *x* axis and temperature dependence of line-width of these phonon modes will give us insight into the spin–phonon coupling in DCO nanoplatelets and it was surprising to see an intense mode at ~429 cm^{-1} as compared to other Raman modes. The Raman mode at ~488 cm^{-1} consists of very complex region involving overlapping and crossing of bands. The presence of these modes is observed for most of the distorted $RCrO_3$ compounds and can be assigned to B_{3g}, A_g and B_{2g} symmetry, respectively. This symmetry allows the crossing of modes resulting into single mode with same frequency at ~488 cm^{-1} as observed for the DCO nanoplatelets. The sharp peak around ~550 cm^{-1} mainly involves stretching vibration (B_{3g}) of the CrO_6 octahedra. The phonon-mode at ~610 cm^{-1} involves the in-phase O_2 stretching (B_{2g}). It is interesting to note that in our study, we also found a peak in high frequency region *i.e.* near 707 cm^{-1} which can be assigned to defect caused in the CrO_6 octahedra by Dy^{3+} cations. Raman spectrum (Fig. 1) for the present DCO sample looks analogous to the spectra reported for bulk DCO.[38]

In order to see the origin of Raman active modes and to better understand the signature of magnetic transition and origin of ferroelectricity, Raman spectra of the DCO nanoplatelets were investigated in a temperature range 93–273 K (Fig. 2(a)). As seen from the Fig. 2(b), following changes can be noticed in the spectra: (1) an increase in the intensity of all the major peaks was observed after cooling from 300 K to 153 K which decreases further at 123 K and 93 K, respectively, (Fig. 2(b) inset) (2) higher wave-number peaks become broader as they reach Nèel temperature (T_N ~ 143 K). The above observations can be explained by considering the anharmonic effect of the lattice and shift in peak position can be accounted for the change in oxygen and cation bond length.[39]

Raman line-widths are closely associated with the phonon lifetime and hence spin–phonon coupling. The temperature dependence of line-width of (a) in-phase and (b) out-of-phase octahedral rotation (265 cm^{-1} and 300 cm^{-1}) in temperature range 93–273 K is plotted in Fig. 3. We observe an anomaly near ~T_N (143 K) for both in-phase and out-of-phase octahedral

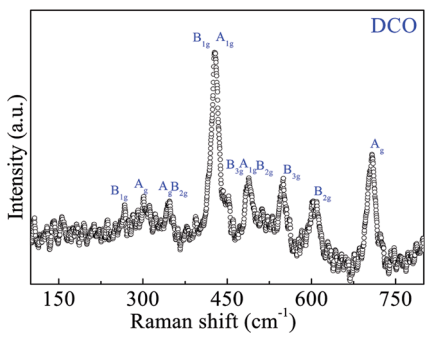

Fig. 1 Room temperature Raman spectra of DCO nanoplatelets.

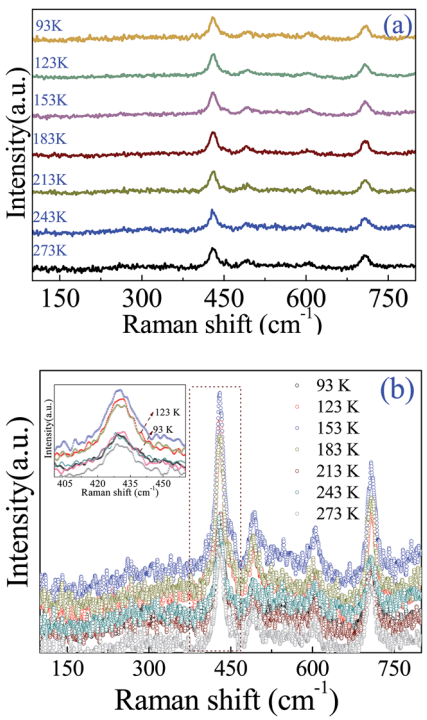

Fig. 2 (a and b) Temperature dependent Raman spectra of DCO nanoplatelets in a temperature range 93–273 K. Inset of (b) showing the change in peak intensity with respect to temperature.

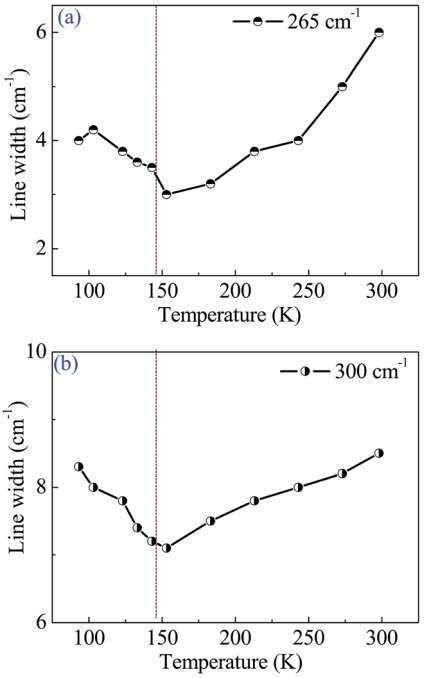

Fig. 3 Temperature dependence on phonon line width of (a) B_{1g} and (b) A_g mode (265 and 300 cm^{-1}) representing in-phase and out of phase octahedral rotation in DCO nanoplatelets.

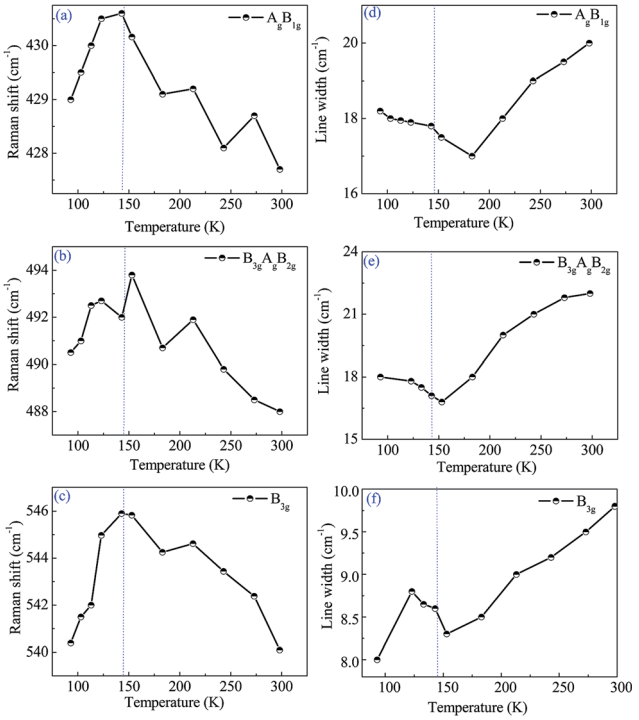

Fig. 4 Temperature dependence of phonon frequency and corresponding line width of phonon modes at (a and d) 429 cm^{-1}, (b and e) 485 cm^{-1}, (c and f) 550 cm^{-1}, respectively. A_{1g} mode (485 cm^{-1}) representing Cr–O vibration in CrO_6 octahedral of DCO nanoplatelets.

rotation of the CrO_6 octahedral which reflects the tilting of octahedral and its deviation from 180° which is affected by the magnetic interaction of Dy^{3+} and Cr^{3+} spins. Raman line-width tends to decrease with temperature due to anharmonicity but here we observe an increase below T_N signifying the contribution from change in phonon lifetime. This change in phonon lifetime is greatly affected by process such as spin–phonon coupling and electron–phonon coupling.[40]

For a closer inspection, phonon frequencies (429 cm^{-1}, 485 cm^{-1} and 550 cm^{-1}) (Fig. 4(a)–(c)) and their corresponding line widths (Fig. 4(d)–(f)) were plotted in a temperature range ~93–300 K. The Fig. 4(a) reveals the change in Raman spectra in the vicinity of the Nèel temperature ($T_N \sim 143$ K). The mode at 429 cm^{-1} gradually hardens with increasing temperature and shows an anomaly near the T_N. The hardening of the Raman mode is attributed to the thermal contraction while softening of the mode occurs below the T_N; which may be related to different magnetic interaction between Dy^{3+} and Cr^{3+} spins. The anomalous behavior of A_g and B_{1g} modes in the DCO may be due to the combined effect of thermal contraction and spin–phonon coupling. To get a deeper insight into the origin of anomalous behavior of 429 cm^{-1} mode, corresponding line-width with respect to temperature was plotted (Fig. 4(d)). The change in Raman line-width was found to be non-monotonous in the DCO nanocrystallites. An anomalous increase in line-width below ~T_N is mainly due to the change in the phonon lifetime contributing from the spin–phonon coupling.[40] The line-width plot shows a dip near the Nèel temperature and a sudden increase below the T_N, suggesting the contribution from the various processes such as spin–phonon coupling and electron–phonon coupling.[40]

The temperature dependence of Raman mode (B_{3g}, A_g, B_{2g}) at 488 cm^{-1} and their corresponding line-width are shown in Fig. 4(b) and (e). As analyzed, the phonon frequency shows an anomaly at around T_N and a sudden increase in phonon frequency below T_N suggests the change in the phonon lifetime. Moreover, the decrease in line-width till T_N with decrease in temperature can be accounted for the reduction of anharmonic phonon decay in the DCO nanoplatelets and increase in line width below T_N suggesting the presence of spin–phonon coupling.

To verify whether the phonon mode—B_{3g} (550 cm^{-1}) is associated with the stretching vibration mode of CrO_6 octahedra, we analyzed the temperature dependent behavior of phonon frequency and corresponding line width as shown in Fig. 4(c) and (f). Similar to other modes as explained above we have observed an anomaly around the T_N along-with a decrease in the phonon frequency below the T_N suggesting the softening of phonon mode which also demonstrates the Dy-ion displacement due to weak ferromagnetism originated from the Cr-ordering.[40] The displacement of Dy-ion and stretching of CrO_6 octahedra give rise to ferroelectricity in this class of materials. The observed decrease in line-width with decrease in temperature is associated with the reduction of anharmonic phonon decay in the DCO nanoplatelets.[40] The broadening of line-width below T_N in B_{3g} mode also suggest the presence of spin–phonon coupling.

From temperature dependent Raman studies (Fig. 2(b)), we can infer that, in DCO nanoplatelets, the Raman intensity was found to increase till T_N which drops at ~123 K and decreases

further at ~93 K. This behavior can be understood by considering the fact that the CrO_6 octahedra distortion increases and shortened bond results into the enhanced Raman intensity and hardening of Raman frequencies. Also, the anomalous behavior of line-width with the change in temperature can be accounted to the spin–phonon coupling in DCO nanocrystallites.

3.2. Dielectric spectroscopy studies

In order to understand the dielectric response of DCO polycrystallites, frequency and temperature dependent plots of real and imaginary parts of complex permittivity of the DCO nanoplatelets in a temperature range of 20–300 K are shown in Fig. 5. As seen from Fig. 5(a) and (b), the ε' and ε'' values decrease with the increase in frequency. However, at low frequency, dipoles follow the field and the increased value of ε' and ε'' is observed which decreases further as dipoles lag behind the field with the increase in frequency. At low frequency, larger values of ε' are mainly due to contribution from the interfacial, dipolar, atomic, ionic and electronic polarization and can be explained by the Maxwell–Wagner effect.[41] The higher value of dielectric constant can be accounted to the conduction in the grain and grain boundary of the material as they are separated by the insulating intergrain barriers.[40] Moreover, with the increase in the temperature from 20 K to 300 K, the dipoles overcome the thermal barrier and orients themselves in the field direction giving larger value of dielectric constant as shown in Fig. 5(a) and (b).[42,43] The temperature dependence of ε' and ε'' at different frequencies also show the increasing trend in the dielectric constant value with the increase in temperature till 300 K as shown in Fig. 5(c) and (d). However, below 100 K, the ε' and ε'' values show a plateau (inset of Fig. 5(c)) above which the gradual increase is observed with an anomaly at ~144 K (T_N) suggesting a weak coupling between the magnetic and electric ordering. Unlike ferroelectric transitions, the dielectric anomalies at magnetic transition temperature are far weaker and they might arise due to the weak magnetoelectric coupling.[43] Above 150 K, the dielectric permittivity values increase further at higher temperature. The ε' and ε'' values strongly depend on the frequency and they increase with the decrease in frequency. Similar behavior was observed in the (Fig. 5(a) and (b)) frequency spectrum also.

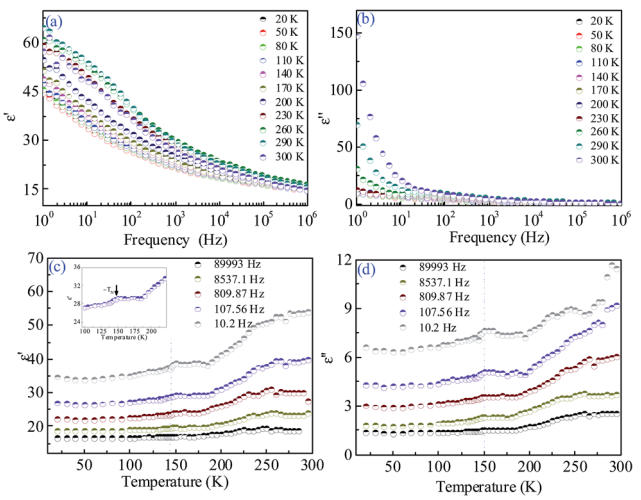

Fig. 5 Frequency and temperature dependence of (a and c) real part (b and d) imaginary part of permittivity value in a temperature range 20–300 K for DCO nanoplatelets.

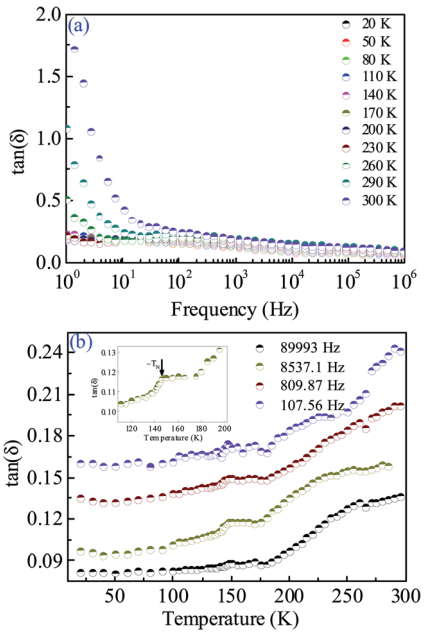

Fig. 6 (a) Temperature dependent of dielectric loss (tan δ) value at different frequency and (b) frequency dependent dielectric loss in a temperature range 10–300 K showing an anomaly at T_N ~ 143 K for DCO nanoplatelets. Inset shows the zoomed view at ~T_N.

The variation of dielectric loss (tan δ) with frequency at different temperatures is shown in Fig. 6(a). The dielectric loss value increases at low frequency and *vice versa* giving flatness at higher frequency. The tan δ value increases after certain temperature, as dipoles no longer follow the field direction. It can be seen from the figure that there is a knee above ~10^4 Hz followed by an increase in loss value. We see a clear peak in the plot (Fig. 6(b)) of temperature dependent dielectric loss at ~144 K in close proximity with the magnetic transition (T_N) (inset of Fig. 6(b)) suggesting the weak coupling between electric and magnetic order parameter.

3.3. UV-visible spectroscopy

Prior to investigate the photocatalytic activity, it is essential to study the optical absorption of the DCO nanoplatelets as the UV-vis absorption edge is relevant to the band energy. Fig. 7(a) shows the UV-visible absorption spectra of the DCO nanoplatelets. In rare earth chromites, the energy states consist of R^{3+}: 4f levels, filled O^{2-}: 2p band, partially filled Cr^{3+}: 3d, empty Cr^{3+}: 4s band and R^{2+}: $4f^{n+1}$ levels or extremely narrow bands.[44] In a similar fashion, Dy^{3+} ions have half-filled $4f^7$ electronic configuration and can have 4f–4f, 4f–5d transition. It can also be associated with charge transfer transitions. The transitions involving 4f–5d and charge transfer cannot be detected due to

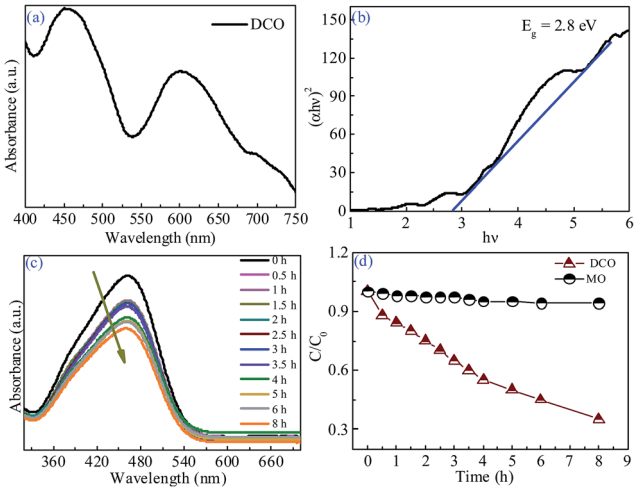

Fig. 7 (a) UV-Vis absorption spectra and (b) band edge energy of DCO nanoplatelets. (c) UV-Vis absorption spectra and (d) photodegradation efficiency of MO as a function of irradiation time under UV light by DCO nanoplatelets.

the limitation of our instrument as it appears at much higher energies. The absorption spectra of DCO show two peaks at ~455 nm and ~603 nm which can be attributed to the $^4A_2$ to $^4T_2$ and $^4T_1$ transitions, respectively. The observed transition can be explained by considering octahedral crystal field splitting.[45–47] The 4f level splits into singlet ground state ($^4A_2$) and triplet excited state ($^4T_2$ and $^4T_1$).[44,45] The presence of Cr^{3+} centers in DCO gives the light green color to the material.[44] The bands at ~455 nm and ~603 nm, are associated with vibrational transitions of Cr^{3+} ion.[47] The observed bands can also be assigned due to the Zeeman splitting of an excited electron due to the local field of Dy^{3+} ion. The bandgap of the DCO nanoplatelets is calculated from the tangent line in the plot of $(\alpha h\nu)^2$ against $h\nu$ (where α is absorption coefficient and $h\nu$ is photon energy) and found to be ~2.8 eV as shown in Fig. 7(b). Thus, the band gap obtained for the DCO nanoplatelets indicates towards the possibility of utilizing UV-vis light for photocatalysis. However, perovskites such as bismuth ferrite (BFO) have been studied a lot for their photocatalytic activity as the band gap of BFO could be tuned from ~1.82 to ~2.27 eV for different morphologies.[48]

3.4. Photocatalytic activity

The photocatalytic activity of the DCO nanoplatelets was evaluated by the degradation of the methyl orange (MO) under UV illumination. The sequential evolution of the spectral changes taking place during the photodegradation of MO with DCO nanoplatelets is displayed in Fig. 7(c) and time-dependent photodegradation is illustrated in Fig. 7(d). The suspensions were magnetically stirred in dark for ~4 h to achieve the adsorption–desorption equilibrium between photocatalyst and MO. The degradation of MO without photocatalyst under UV light is extremely slow and only 4% MO was degraded after 8 h illumination. However, in presence of DCO as photocatalyst, the rate of MO degradation increased to 55% after 6 h UV irradiation. After 8 h UV-vis irradiation with DCO, the MO degradation rate was saturated to about 65%. The plausible explanation for efficient degradation of MO using DCO as a catalyst can be understood by considering DCO as a semiconductor rather than insulator.[25] The rare earth chromites are known as p-type semiconductor due to the conduction of holes from Cr^{4+} to Cr^{3+} centers. Owing to the native defects in $RCrO_3$, there exist a Cr^{4+} centers and presence of these defects results in enhance conduction of electrons which in due course increases the formation of OH^- radical responsible for MO degradation efficiently.[44] From these studies, we can infer that DCO can be used as a potential photocatalyst.

4. Conclusions

In conclusion, Raman spectroscopy has provided significant information on the lattice-distortion and their variation with temperature. The temperature dependent Raman spectra of the DCO nanoplatelets and associated phonon-modes provide a better understanding of structural investigation in the DCO nanoplatelets. Our results clearly demonstrate that the interplay between spin and lattice indicating spin–phonon coupling and softening of the phonon modes in the DCO nanoplatelets. The observed anomalies around Nèel temperature for all the modes illustrate the possible spin–phonon coupling in the DCO nanoplatelets. A weak magnetoelectric coupling is observed for the DCO nanoplatelets by impedance spectroscopic studies, showing a signature in the vicinity of the Nèel transition. The band-edge information of the DCO nanoplatelets raised a probability of using it as a photocatalyst. The DCO nanoplatelets were found to be an efficient photocatalyst in degrading the MO to 65% after 8 h UV illumination. However, based on the band gap information and position of reduction potential for water, it can be expected that the DCO can also be used for water splitting under UV-visible light irradiation. If the reduction potential for water is below the conduction band minimum of DCO, then the material possess great prospective for H_2 evolution from water under UV-visible light irradiation. Moreover, in context to above, all other rare earth chromites can also be used as a promising candidate for photocatalysis, which needs to be studied in future.

Acknowledgements

P.P acknowledges support from Young Scientist Award grant from Council for Scientific and Industrial Research (CSIR) in Physical Sciences and a separate grant from Department of Science & Technology (DST), India (DST/INT/ISR/P-8/2011). P.P also acknowledges center of excellence of surface science and CSIR-Network programme of Nano-safety, health, and environment. P.G acknowledges the support from the Council of Scientific and Industrial Research (CSIR), India for providing Senior Research Fellowship (SRF).

References

1 D. Khomskii, Classifying multiferroics: Mechanisms and effects, *Physics*, 2009, **2**, 20.

2 C. N. R. Rao and C. R. Serrao, New routes to multiferroics, *J. Mater. Chem.*, 2007, **17**, 4931–4938.
3 T. Arima, A. Tokunaga, T. Goto, H. Kimura, Y. Noda and Y. Tokura, Collinear to Spiral Spin Transformation without Changing the Modulation Wavelength upon Ferroelectric Transition in $Tb_{1-x}Dy_xMnO_3$, *Phys. Rev. Lett.*, 2006, **96**, 097202.
4 W. Eerenstein, N. D. Mathur and J. F. Scott, Multiferroic and magnetoelectric materials, *Nature*, 2006, **442**, 759.
5 M. Fiebig, T. Lottermoser, D. Frohlich, A. V. Goltsev and R. V. Pisarev, Observation of coupled magnetic and electric domains, *Nature*, 2002, **419**, 818.
6 M. C. Weber, J. Kreisel, P. A. Thomas, M. Newton, K. Sardar and R. I. Walton, Phonon Raman scattering of $RCrO_3$ perovskites (R = Y, La, Pr, Sm, Gd, Dy, Ho, Yb, Lu), *Phys. Rev. B: Condens. Matter Mater. Phys.*, 2012, **85**, 054303.
7 S. M. Feng, L. J. Wang, J. L. Zhu, F. Y. Li, R. C. Yu, C. Q. Jin, X. H. Wang and L. T. Li, Pressure-induced phase transition in $Ho_{0.8}Dy_{0.2}MnO_3$ multiferroic compound, *J. Appl. Phys.*, 2008, **103**, 026102.
8 A. Jaiswal, R. Das, K. Vivekanand, T. Maity, P. M. Abraham, S. Adyanthaya and P. Poddar, Magnetic and dielectric properties and Raman spectroscopy of $GdCrO_3$ nanoparticles, *J. Appl. Phys.*, 2010, **107**, 013912.
9 E. F. Bertaut, J. Marescha, G. Devries, R. Aleonard, R. Pauthene, J. Rebouill and V. Zarubick, *IEEE Trans. Magn.*, 1966, **MAG2**, 453.
10 K. Tsushima, K. Aoyagi and S. Sugano, Magnetic and Magneto-Optical Properties of Some Rare-Earth and Yttrium Orthochromites, *J. Appl. Phys.*, 1970, **41**, 1238.
11 K. Sardar, M. R. Lees, R. J. Kashtiban, J. Sloan and R. I. Walton, Direct Hydrothermal Synthesis and Physical Properties of Rare-Earth and Yttrium Orthochromite Perovskites, *Chem. Mater.*, 2011, **23**, 48.
12 Y. L. Su, J. C. Zhang, L. Li, Z. J. Feng, B. Z. Li, Y. Zhou and S. X. Cao, Novel Magnetization Induced by Phase Coexistence in Multiferroic $HoCrO_3$ Chromites, *Ferroelectrics*, 2010, **410**, 102.
13 J. R. Sahu, C. R. Serrao, N. Ray, U. V. Waghmare and C. N. R. Rao, Rare earth chromites: a new family of multiferroics, *J. Mater. Chem.*, 2007, **17**, 42.
14 C. R. Serrao, A. K. Kundu, S. B. Krupanidhi, U. V. Waghmare and C. N. R. Rao, Biferroic $YCrO_3$, *Phys. Rev. B: Condens. Matter Mater. Phys.*, 2005, **72**, 220101.
15 A. Durán, A. M. Arévalo-López, E. Castillo-Martínez, M. García-Guaderrama, E. Moran, M. P. Cruz, F. Fernández and M. A. Alario-Franco, Magneto-thermal and dielectric properties of biferroic $YCrO_3$ prepared by combustion synthesis, *J. Solid State Chem.*, 2010, **183**, 1863.
16 Z. X. Cheng, X. L. Wang, S. X. Dou, H. Kimura and K. Ozawa, A novel multiferroic system: Rare earth chromates, *J. Appl. Phys.*, 2010, **107**, 09D905.
17 N. D. Todorov, M. V. Abrashev, V. G. Ivanov, G. G. Tsutsumanova, V. Marinova, Y. Q. Wang and M. N. Iliev, Comparative Raman study of isostructural $YCrO_3$ and $YMnO_3$: Effects of structural distortions and twinning, *Phys. Rev. B: Condens. Matter Mater. Phys.*, 2011, **83**, 224303.
18 M. N. Iliev, A. P. Litvinchuk, V. G. Hadjiev, Y. Q. Wang, J. Cmaidalka, R. L. Meng, Y. Y. Sun, N. Kolev and M. V. Abrashev, Raman spectroscopy of low-temperature (*Pnma*) and high-temperature ($R\bar{3}$ phases of $LaCrO_3$, *Phys. Rev. B: Condens. Matter Mater. Phys.*, 2006, **74**, 214301.
19 M. Udagawa, K. Kohn, N. Koshizuka, T. Tsushima and K. Tsushima, Influence on magnetic ordering on the phonon Raman spectra in $YCrO_3$ and $GdCrO_3$, *Solid State Commun.*, 1975, **16**, 779.
20 D. Ullrich, R. Courths and C. Grundherr, Magnetic ordering and phonon Raman spectra of $ErCrO_3$, *Physica B+C*, 1977, **89**, 205.
21 W. Kaczmarek and I. Morke, Raman scattering and the antiferromagnetic phase transition in $HoCrO_3$, *J. Magn. Magn. Mater.*, 1986, **58**, 91.
22 Y. Du, Z. X. Cheng, X. L. Wang and S. X. Dou, Structure, magnetic, and thermal properties of $Nd_{1-x}La_xCrO_3$ ($0 \leq x \leq 1.0$), *J. Appl. Phys.*, 2010, **108**, 093914.
23 B. Rajeswaran, D. I. Khomskii, A. K. Zvezdin, C. N. R. Rao and A. Sundaresan, Field-induced polar order at the Nèel temperature of chromium in rare-earth orthochromites: interplay of rare-earth and Cr magnetism, *Phys. Rev. B: Condens. Matter Mater. Phys.*, 2012, **86**, 214409.
24 J. Prado-Gonjal, R. Schmidt, J.-J. Romero, D. Ávila, U. Amador and E. Morán, Microwave-Assisted Synthesis, Microstructure, and Physical Properties of Rare-Earth Chromites, *Inorg. Chem.*, 2013, **52**, 313.
25 G. V. Rao Subba, B. M. Wanklyn and C. N. R. Rao, Electrical Transport in Rare Earth Ortho-chromites, Manganites and Ferrites, *J. Phys. Chem. Solids*, 1971, **32**, 345.
26 F. Gao, X. Chen, K. Yin, S. Dong, Z. Ren, F. Yuan, T. Yu, Z. Zou and J.-M. Liu, Visible-Light Photocatalytic Properties of Weak Magnetic $BiFeO_3$ Nanoparticles, *Adv. Mater.*, 2007, **19**, 2889.
27 M. Siemons and U. Simon, High throughput screening of the propylene and ethanol sensing properties of rare-earth orthoferrites and orthochromites, *Sens. Actuators, B*, 2007, **126**, 181.
28 N. Russo, D. Mescia, D. Fino, G. Saracco and V. Specchia, N_2O Decomposition over Perovskite Catalysts, *Ind. Eng. Chem. Res.*, 2007, **46**, 4226; D. Lakshmi and R. Sundaram, Humidity sensor studies on $Dy_{1-x}Sr_xCrO_3$ (0×0.1) synthesized by microwave assisted combustion method, *Sens. Transducers J.*, 2008, **97**, 74.
29 J. W. Fergus, Lanthanum chromite-based materials for solid oxide fuel cell interconnects, *Solid State Ionics*, 2004, **171**, 1; G. A. Tompsett and N. M. Sammes, *J. Power Sources*, 2004, **130**, 1.
30 J. Beckers and G. Rothenberg, "Hot Spot" Hydrocarbon Oxidation Catalysed by Doped Perovskites—Towards Cleaner Diesel Power, *ChemPhysChem*, 2005, **6**, 223.
31 A. L. Linsebigler, G. Lu and T. Yates John, Photocatalysis on TiOn Surfaces: Principles, Mechanisms, and Selected Results, *Chem. Rev.*, 1995, **95**, 735.

32 P. Gupta, R. Bhargava, R. Das and P. Poddar, Static and dynamic magnetic properties and effect of surface chemistry on the morphology and crystallinity of $DyCrO_3$ nanoplatelets, *RSC Adv.*, 2013, **3**, 26427.

33 M. N. Iliev, M. V. Abrashev, H. G. Lee, V. N. Popov, Y. Y. Sun, C. Thomsen, R. L. Meng and C. W. Chu, Raman spectroscopy of orthorhombic perovskite like $YMnO_3$ and $LaMnO_3$, *Phys. Rev. B: Condens. Matter Mater. Phys.*, 1998, **57**, 2872.

34 M. V. Abrashev, J. Bäckström, L. Börjesson, V. N. Popov, R. A. Chakalov, N. Kolev, R. L. Meng and M. N. Iliev, Raman spectroscopy of $CaMnO_3$: Mode assignment and relationship between Raman line intensities and structural distortions, *Phys. Rev. B: Condens. Matter Mater. Phys.*, 2002, **65**, 184301.

35 M. Fiebig, Revival of the magnetoelectric effect, *J. Phys. D: Appl. Phys.*, 2005, **38**, R123.

36 M. N. Iliev, M. V. Abrashev, J. Laverdiére, S. Jandl, M. M. Gospodinov, Y. Q. Wang and Y. Y. Sun, Distortion-dependent Raman spectra and mode mixing in $RMnO_3$ perovskites (R = La, Pr, Nd, Sm, Eu, Gd, Tb, Dy, Ho, Y), *Phys. Rev. B: Condens. Matter Mater. Phys.*, 2006, **73**, 064302.

37 J. Laverdière, S. Jandl, A. A. Mukhin, V. Y. Ivanov, V. G. Ivanov and M. N. Iliev, Spin–phonon coupling in orthorhombic $RMnO_3$ (R = Pr, Nd, Sm, Eu, Gd, Tb, Dy, Ho, Y): A Raman study, *Phys. Rev. B: Condens. Matter Mater. Phys.*, 2006, **73**, 214301.

38 A. Mc Dannald, L. Kuna and M. Jain, Magnetic and magnetocaloric properties of bulk dysprosium chromite, *J. Appl. Phys.*, 2013, **114**, 113904.

39 D. Rout, K. S. Moon and S. J. L. Kang, Temperature-dependent Raman scattering studies of polycrystalline $BiFeO_3$ bulk ceramics, *J. Raman Spectrosc.*, 2009, **40**, 618.

40 V. Bhadram, B. Rajeswaran, A. Sundaresan and C. Narayana, Spin–phonon coupling in multiferroic $RCrO_3$ (R-Y, Lu, Gd, Eu, Sm): A Raman study, *EPL*, 2013, **101**, 17008.

41 U. Intatha, S. Eitssayeam, J. Wang and T. Tunkasiri, Impedance Study of Giant Dielectric Permittivity in $BaFe_{0.5}Nb_{0.5}O_3$ Perovskite Ceramic, *Curr. Appl. Phys.*, 2010, **10**, 21.

42 A. Jaiswal, R. Das, T. Maity and P. Poddar, Dielectric and spin relaxation behaviour in $DyFeO_3$ nanocrystals, *J. Appl. Phys.*, 2011, **110**, 124301.

43 A. Jaiswal, R. Das, T. Maity, K. Vivekanand, S. Adyanthaya and P. Poddar, Temperature-Dependent Raman and Dielectric Spectroscopy of $BiFeO_3$ Nanoparticles: Signatures of Spin–Phonon and Magnetoelectric Coupling, *J. Phys. Chem. C*, 2010, **114**, 12432–12439.

44 A. K. Tripathi and H. B. Lal, Electrical transport in light rare-earth orthochromites, *J. Mater. Sci.*, 1982, **17**, 1595–1609.

45 R. Bhatt, S. Kar, K. S. Bartwal and V. K. Wadhawan, The effect of Cr doping on optical and photoluminescence properties of $LiNbO_3$ crystals, *Solid State Commun.*, 2003, **127**, 457.

46 A. Jaiswal, R. Das, S. Adyanthaya and P. Poddar, Synthesis and optical studies of $GdCrO_3$ nanoparticles, *J Nanopart. Res.*, 2011, **13**, 1019.

47 G. A. Torchia, J. A. Munoz, F. Cusso, F. Jaque and T. O. Toch, The luminescent quantum efficiency of Cr^{3+} ions in co-doped crystals of $LiNbO_3$:ZnO determined by simultaneous multiple-wavelength photoacoustic and luminescence experiments, *J. Lumin.*, 2001, **92**, 317.

48 S. Li, Y.-H. Lin, B.-P. Zhang, Y. Wang and C.-W. Nan, Controlled Fabrication of $BiFeO_3$ Uniform Microcrystals and Their Magnetic and Photocatalytic Behaviors, *J. Phys. Chem. C*, 2010, **114**, 2903.